Chaotic dynamics in classical *s*-wave helium

Zai-Qiao Bai and Yan Gu
Department of Astronomy and Applied Physics, Center of Nonlinear Science, University of Science and Technology of China, Hefei, Anhui 230026, China
(Received 10 December 1998)

Classical dynamics of *s*-wave helium in the case of $E<0$ is investigated by the geometric method. The ambiguousness of the orbits after two-electron critical collision (TECC) is eliminated by confining the motion to the fundamental domain defined by $r_1>r_2$. Scattering orbits are classified into undelayed and delayed (resonant) according to whether they can avoid the recurrence of reaction. A global Smale horseshoe on the surface of section is constructed for the case of $Z=2$ which implies that the bounded motion is purely chaotic and explains the onset of the chaotic (resonant) scattering when the incident energy is below a threshold. Immediately below the threshold, the probability of resonant scattering increases linearly with the energy difference. Moreover, we found that the permitted code sequences for the scattering orbits at a given incident energy are determined by the principal TECC orbit. Compared with the e^-Ze^- collinear helium, the *s*-wave helium is less chaotic and exhibits a more intricate threshold behavior. [S1063-651X(99)06509-5]

PACS number(s): 05.45.−a, 45.05.+x

I. INTRODUCTION

As one of the most important examples of a nonintegrable Hamiltonian system as well as a semiclassical approach to the strongly correlated motion in two-electron atoms or ions, the classical dynamics of three-body Coulomb system has been attracting increasing attention in recent years [1–14,17]. However, being complicated by its multidimensional, nonseparable and nonperturbative nature, the problem still remains a challenge for physicists [5]. Thus far, several simplified models have been proposed, among them, the *s*-wave helium, where the two electrons are restricted to spherical states with individual angular momentum equal to zero, is one of the most physically transparent models. In this model, it is found that the bounded motion is purely chaotic while almost all initial points will lead to the escape of one electron, i.e., autoionization, and the lifetime distribution induces a fractal structure on phase space [12], which are very similar to the phenomena observed in the numerical studies on the coplanar three-body Coulomb systems [8,9]. In addition, quantum calculations of bounded as well as scattering states based on this model have also yielded reasonable results [15,16]. All these facts give hope that the essential physics of the original system is well preserved in this simplified model.

Despite the many important and interesting phenomena discovered in the classical *s*-wave helium, a direct account of the global dynamics of this system, especially its dependence upon the nuclear charge number *Z*, is still lacking. In this paper we shall investigate the *s*-wave Coulomb three-body system by geometrical methods so as to understand all its important global properties. In order to eliminate the discontinuity at two-electron critical collisions, we take advantage of the electron exchange symmetry of the system and study its motion in the fundamental domain. Then there comes a category of critical *e*-*e* collision orbits which are crucial to the understanding of the qualitative dynamics of the system. Special attention is also paid to the critical escape and critical injection orbits, which play an important role in the unbounded many-body systems [17,18].

The paper is organized in the following way: We introduce in the next section the motion of *s*-wave helium in the fundamental domain and a code system which is appropriate for a symbolic description of the orbits. In Sec. III, we give a comprehensive account of the global behaviors in the case of $E<0$, which includes the Smale horseshoe and the accompanying symbolic dynamics, the tilling of the surface of section (SOS) by the escape and injection regions and the classification of scattering orbits. This is followed by a general discussion and a brief summary.

II. PRELIMINARY

A. Critical collision between electrons

In the *s*-wave model, a two-electron atom or ion is described as two spherical shells of charge -1 expanding and contracting around a fixed nucleus of charge *Z*. The Hamiltonian of this model in atomic units can be written as [12]

$$H=\frac{1}{2}(p_1^2+p_2^2)-\frac{Z}{r_<}-\frac{Z-1}{r_>},$$

where $r_<=\min\{r_1,r_2\}$ and $r_>=\max\{r_1,r_2\}$ with $r_i\geqslant 0$ and p_i being coordinate and momentum of ith electron ($i=1,2$). As compared with other restricted helium models, the *s*-wave model exhibits the simplest dynamics in the sense that the two electrons are actually uncoupled between their two consecutive encounters, so that the energy of each electron, i.e., $E_1=\frac{1}{2}p_1^2-(Z-1)/r_1$, $E_2=\frac{1}{2}p_2^2-Z/r_2$ if $r_1>r_2$ or $E_1=\frac{1}{2}p_1^2-Z/r_1$, $E_2=\frac{1}{2}p_2^2-(Z-1)/r_2$ if $r_2>r_1$, keeps, for the most time, constant. The *e*-*e* interaction takes place when the two electrons collide at $r_1=r_2=\rho$, where the energy could be transferred between the two electrons. As a result, only the total energy $E=E_1+E_2$ is a global constant of motion. Furthermore, the homogeneous potential implies a scaling symmetry (similarity principle), by which we can scale *E* to -1 as we consider only the case of negative total energy in this paper [19].

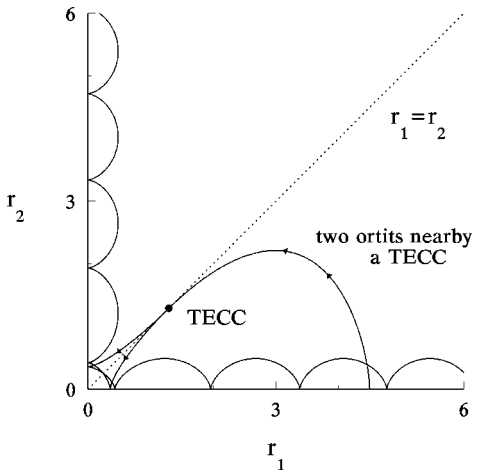

FIG. 1. Two orbits which pass near a TECC. They are symmetric with respect to the Wannier ridge $r_1=r_2$ (dashed line) after approaching the TECC.

An *e-e* collision can be labeled by (p_1,p_2), the momentums of the two electrons immediately before it occurs or, alternatively, by $(P_1,P_2)\equiv(\sqrt{\rho}p_1,\sqrt{\rho}p_2)$ for convenience. Then all events of *e-e* collision are represented in the (P_1,P_2) plane by an open disk defined by the energy relation $P_1^2+P_2^2=2(2Z-1-\rho)<2(2Z-1)$. Among these collisions, there exists a special category characterized by $P_1=P_2=P_c$, each of them we call a two-electron critical collision (TECC).

The motion at a TECC is not continuous, i.e., starting immediately before it with $r_1=r_2+0$ and $p_1=p_2\mp 0$ will thereafter lead to two orbits which are symmetric with respect to the line of $r_1=r_2$ (see Fig. 1). However, if we take advantage of the electron exchange symmetry and study the motion in the fundamental domain (FD) defined by $r_1>r_2$ [4], this ambiguity can be eliminated. By setting an elastically reflection wall at $r_1=r_2$, $e_1(e_2)$ will always be the outer(inner) electron and an orbit can be unambiguously continued after a TECC.

Note that the symmetric motion of the electron pair on the Wannier ridge $(r_1=r_2)$ is excluded from the dynamics. The reason is that the Wannier orbit (if it exists in *s*-wave helium) is isolated on the steep ridge and cannot be approached by its nearby orbits. Instead of the Wannier orbit, we have a category of TECC orbits, which play an important role in understanding the qualitative behavior of the *s*-wave model as it will be shown latter.

B. Surface of section and the symbolic description of orbits

By using the Poincaré section method, the dynamics is reduced to a two-dimensional mapping. The surface of section can be set at $r_2=0$, i.e., at the collision between the inner electron and the nucleus. To eliminate the divergence of p_1 when $r_1\to 0$, the coordinates $(R,P)=(\sqrt{r_1},\sqrt{r_1}p_1)$ on SOS are used, in terms of which the mapping is area preserving.

A symbolic method can be used to give a qualitative description of the dynamics. Since an arbitrary orbit, bounded as well as unbounded, will cross SOS for infinitely many times, each orbit can be divided into infinitely many segments by the points of intersection. As between two consecutive crossings of SOS, an orbit can attain the ridge of the potential at $r_1=r_2$ (i.e., lead to an *e-e* collision) at most once, we assign a code $-$ or $+$ to the segment when there is an or no *e-e* collision. Besides these two general cases, we give a c (which can be regarded as the degenerated $-$ and $+$) to the critical situation when a TECC occurs. In this extended binary code system, an orbit is represented by a bi-infinite symbolic sequence made up from the codes of its sequential segments

$$\cdots\sigma_{-2}\sigma_{-1}\sigma_0\sigma_1\cdots,$$

where $\sigma_i\in\{+,-,c\}$, $i\in Z$. We add a $\bullet$ to this sequence, i.e.,

$$\cdots\sigma_{-2}\sigma_{-1}\bullet\sigma_0\sigma_1\cdots,$$

to mark the present point of this orbit on SOS. Then the action of the Poincaré mapping F (or F^{-1}) manifests itself as a right-shift (or left-shift) of $\bullet$ in the corresponding code sequence. Moreover, we denote $\mathcal{U}(\Sigma)$ the region on SOS where all the points share a common segment of symbolic sequence Σ (with $\bullet$).

III. GLOBAL DYNAMICS

A. General consideration

It is found that the motion in the case of $E\geqslant 0$ is qualitatively simple. All the orbits are initiated from one or two electron(s) injection and terminated at the ionization of one or both electron(s) after a brief time of coupled motion, which we call a reaction, near the nucleus [13]. In the case of $E<0$, however, the recurrence of reaction may occur and, consequently, the system will exhibit a more complicated dynamics.

Consider an injecting orbit initiated with $E_1=E_1^0>0$, $p_1<0$, and $E_2=E_2^0<-E_1^0$. The reaction begins at $t=t_0$ when e_1 first collides e_2 at $r_1=r_2=\rho$ where we have $p_1\leqslant p_2$. If $p_2<0$, then both electrons will move inwards until the inner one collides with the nucleus and turns back, which will lead to an additional *e-e* collision at $r_1=r_2=\rho'$ with $\rho'<\rho$. Then we have $E_1=E_1^0+1/\rho'-1/\rho>E_1^0$ and $p_1>|p_2|$, which enables the outer electron immediately escape to the infinity. In other words, an initial head-to-tail *e-e* collision will always result in a direct scattering [as we consider the motion in FD, direct(exchange) scattering actually means a scattering with even(odd) *e-e* collisions] and the outgoing energy is always greater than the incident energy. Moreover, simple calculations show that the first *e-e* collision always happens at $r_1=r_2=\rho\geqslant\rho_{c1}=1/(E_1^0-E_2^0)$, and we shall have a TECC [i.e., $p_1(t_0)=p_2(t_0)$] if and only if $\rho=\rho_{c1}$.

If $p_2(t_0)>0$, however, the outcome is more complex. From the viewpoint of continuity, if e_2 is sufficiently near to its return point at t_0, i.e., $\rho\approx Z/|E_2^0|$, the orbit will also lead to direct scattering. On the other hand, if ρ is too small and the momentum transferred between the two electrons is sufficiently large, the outer electron will be directly knocked out after the first *e-e* collision and an exchange scattering will occur. We denote the two regions which immediately lead to direct and exchange scatterings by $\rho\geqslant\rho_{c2}$ and $\rho\leqslant\rho_{c3}$, respectively. In Sec. III G, we shall show that $\rho_{c2}=\rho_{c3}$ if ε_i

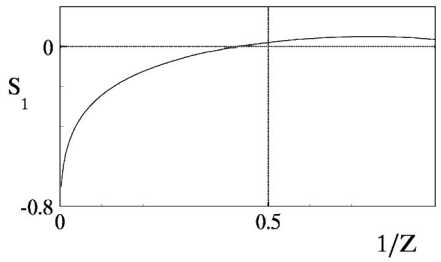

FIG. 2. The dependence of s_1 upon the charge number Z.

$=|E_1^0/E_2^0| \geqslant \varepsilon_{ic}$ (≈ 0.809417 for $Z=2$) and for such initial conditions all the orbits will be ended in the escape of the outer electron after the first reaction and the scattering is as regular as that in the case of non-negative total energy. However, if $\varepsilon_i < \varepsilon_{ic}$, ρ_{c3} will be less than ρ_{c2} and when $\rho \in (\rho_{c3}, \rho_{c2})$, the outer electron cannot escape to the infinity ($E_1 < 0$) after the first reaction and an additional reaction is inevitable due to the reinjection of the outgoing electron. Actually, the iteration of this process will result in chaotic scattering.

Based on the above discussion, the unbounded orbits in the case of $E<0$ can be categorized into two classes, i.e., undelayed (or fast) and delayed (or resonant) scatterings according whether or not they can avoid the recurrence of reaction. In the former class, there are undelayed direct and exchange scatterings which are coded by $+^\infty - - +^\infty$ and $+^\infty - +^\infty$, respectively. While for the latter class, it has a great diversity of permitted code sequences, corresponding to a multitude of possible patterns for the resonant motion.

B. Symbolic sequences for TECC orbits

All TECC's can be naturally parametrized by $P_1 = P_2 = P_c = s\sqrt{2Z-1}$ with $s \in (-1,1)$. Consider an orbit having TECC with label s. If $s \geqslant s_0 \equiv \sqrt{(2Z-2)/(2Z-1)}$, then after this collision we have $p_1 = p_2 > 0$ and $E_1 \geqslant 0$ and e_1 will immediately escape to the infinity. In addition, $s = s_0$ implies that the energy of the outgoing electron is zero, i.e. a critical escape will occur. On the other hand, if $s \leqslant -s_0$, discussion on the head-to-tail collision in the beginning of this section told us that after such TECC, the outer electron will immediately escape after an additional e-e collision. Since a head-to-tail collision with negative E_1^0 may also lead to the same result, we can find a larger interval $(-1, s_1) \supset (-1, -s_0)$ for the TECC orbits which will escape after one more e-e collision and the energy of the escaping electron becomes zero when $s = s_1$. Numerical study shows that $s_1 > 0$ for $Z=2$ while for the integers $Z>2$, we have $s_1 < 0$ (Fig. 2). As it can be seen later, the sign of s_1 is crucial to the global dynamics of the s-wave model Coulomb three-body systems and we shall consider only the case $Z=2$ in the following discussion. By making use of the time reversal symmetry, the symbolic sequences for the TECC orbits could be summarized as follows;

$$+^\infty - c + ^\infty \quad \text{for} \quad s \in [s_0, 1),$$

$$+^\infty - c\Sigma, \quad s \in (s_1, s_0),$$

$$+^\infty - c - +^\infty, \quad s \in [-s_1, s_1],$$

$$\Sigma c - +^\infty, \quad s \in (-s_0, -s_1),$$

$$+^\infty c - +^\infty, \quad s \in (-1, -s_0],$$

where Σ represents a sequence different from $+^\infty$ and $-+^\infty$. As a result, if an orbit experiences at least two TECC's, i.e., its code sequence contains a segment of $c\Sigma' c$ (Σ' contains only $+$ and $-$), then the former TECC must occur at $s \in (s_1, s_0)$ (outgoing wave) while the latter at $s \in (-s_0, -s_1)$ (incoming wave) and its full sequence must be $+^\infty - c\Sigma' c - +^\infty$, i.e., it is a resonant scattering orbit with only two TECC's. We shall call such an orbit a bicritical collision orbit (BCCO).

C. Partition lines induced by TECC orbits

The TECC orbits will intersect with SOS infinitely many times. We shall denote their first intersection after TECC by $U(1)$ and their last intersection before TECC by $S(1)$. The points on $U(1)$ and $S(1)$ can be labeled by the parameter $s \in (-1,1)$ for the corresponding TECC's and will be denoted as $U(1,s)$ and $S(1,s)$, which are connected by the Poincaré mapping, i.e.,

$$F: S(1,s) \to U(1,s), \quad s \in (-1,1).$$

While the symmetry of time reversal implies

$$S(1,s) = [U(1,-s)]^*,$$

where the asterisk denotes the reflection $(R,P)^* \equiv (R,-P)$.

$S(1)$ and $U(1)$ for $Z=2$ are shown in Fig. 3(a), from which we can see that both their ends approach the boundary $R=0$, i.e.,

$$\lim_{s\to 1} S(1,s) = (0,P'), \quad \lim_{s\to 1} U(1,s) = (0,P''),$$

and the time reversal

$$\lim_{s\to -1} S(1,s) = (0,-P''), \quad \lim_{s\to -1} U(1,s) = (0,-P').$$

Moreover, it can be proved that (see the Appendix)

$$\sqrt{2(Z-1)} < P' < \sqrt{2Z-1} < P'' < 2\sqrt{2Z-1} + \sqrt{2Z}.$$

By using the symbols introduced in Sec. II, we have obviously $U(1) = \mathcal{U}(c\bullet)$ and $S(1) = \mathcal{U}(\bullet c)$. As c marks the critical state in the transition between $+$ and $-$ in the symbolic description of orbits, we can see that both $S(1)$ and $U(1)$ are partition lines on SOS. The region confined within $S(1)$ is $\mathcal{U}(\bullet -)$ while that outside $S(1)$ is $\mathcal{U}(\bullet +)$. $\mathcal{U}(\bullet -)$ is bounded and its measure is $(2Z-1)\pi$, which is proportional to the flux of orbits that hit the reflection wall at $r_1 = r_2$ and can be calculated from the Stokes' lemma, while $\mathcal{U}(\bullet +)$ is unbounded. Similarly, $U(1)$ divides SOS into $\mathcal{U}(-\bullet)$ and $\mathcal{U}(+\bullet)$.

The Poincaré mapping is continuous at $S(1)$, i.e., if point X_i approaches a given point $S(1,s)$, then $X_f = F(X_i)$ will tend to $U(1,s)$. Furthermore, if $X_i \in \mathcal{U}(\bullet +)$, as the orbit connecting X_i and X_f changes smoothly, the tangent map (Jacobian) is also well defined. However, if $X_i \in \mathcal{U}(\bullet -)$, the corresponding orbit will lead a reflection at $r_1 = r_2$, which will

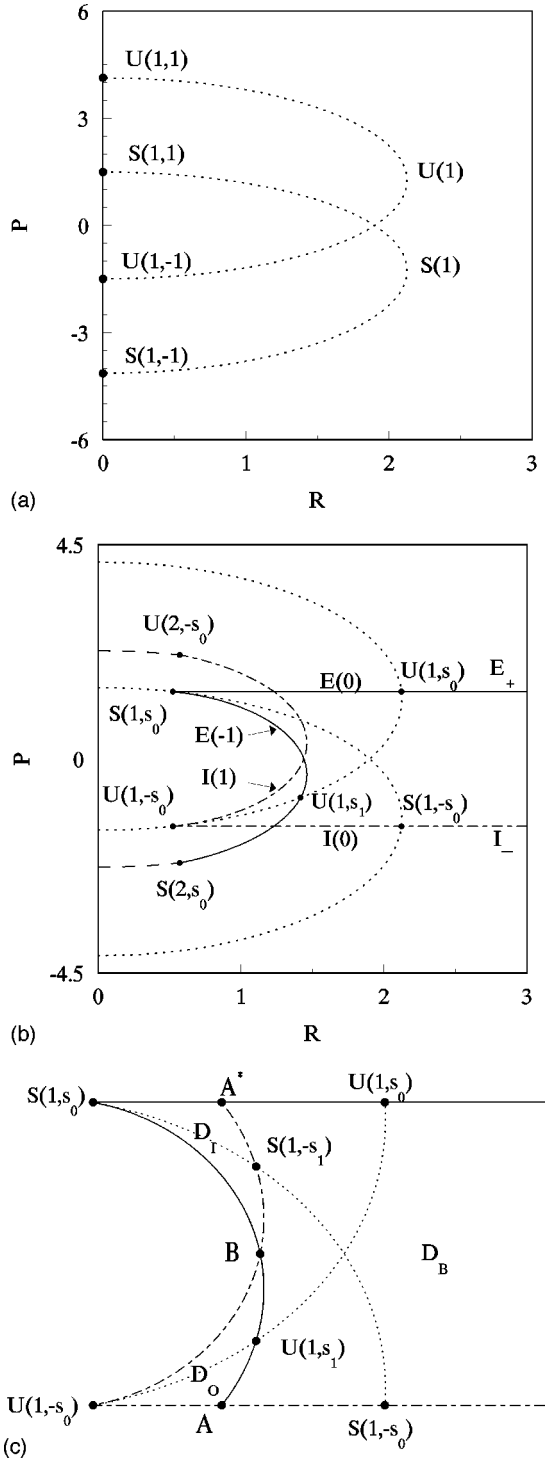

FIG. 3. (a) The partition lines $S(1)$ and $U(1)$ (dotted lines). (b) The resonant zone boundaries (solid lines) E_+, $E(0)$ [from $U(1,s_0)$ to $S(1,s_0)$], and $E(-1)$ [$S(1,s_0)$ to $S(2,s_0)$], and their time reversal (dashed lines) I_-, $I(0)$ [$S(1,-s_0)$ to $U(1,-s_0)$] and $I(1)$ [$U(1,-s_0)$ to $U(2,-s_0)$]. (c) The resonant zone $D=D_I\cup D_o\cup D_B$.

generally cause a variation of orbit to the order of $\delta^{1/2}$ if the deviation of X_i from $S(1,s)$ is of order δ. Hence the Jacobian will generally be singular on $S(1)$. This singularity due to the sudden appearance of reflection explains the folding of a smooth curve that cuts $S(1)$ [or $U(1)$] when mapped by F (or F^{-1}) as we shall frequently see in the following studies. For example, the critical escape line $E(0)\cup E_+$ crosses $U(1)$ at point $U(1,s_0)$ while $F^{-1}[E(0)\cup E_+]=E(-1)\cup E(0)\cup E_+$ shows a cusp at point $S(1,s_0)$ [see Fig. 3(b)].

D. Resonant zone on SOS

The resonant zone, denote it by D, can be so defined on SOS that a scattering orbit is a resonant one if and only if it intersects with SOS within D at least one time. In order to show this zone explicitly, we introduce another set of partition lines related to critical escape and injection.

Consider the region on SOS where the outer electron can immediately escape to infinity, i.e., $\mathcal{U}(\bullet+^{\infty})$. Note that the conditions that $p_1>0$ and $E_1\geqslant 0$ cannot ensure the immediate escape of e_1, i.e., when r_1 is too small, e_2 will move faster than e_1 and may catch up with it despite $E_2<0\leqslant E_1$. Therefore, in this region, E_1 should be greater than a positive threshold so as to prevent the unwanted encounter with e_2. The lower boundary of $\mathcal{U}(\bullet+^{\infty})$ can be determined as follows. In the region where R is sufficiently large, the boundary is the horizontal line of $P=\sqrt{2(Z-1)}$, where $E_1=0$ and $p_1>0$. This straight boundary can be extended to the small R region until it crosses $U(1)$ at $U(1,s_0)$ and ends at $S(1,s_0)$ on $S(1)$. Then $S(1,s)$ with $s\in(s_0,1)$ forms another piece of lower boundary of $\mathcal{U}(\bullet+^{\infty})$ where R is so small that a positive threshold for escape energy exists [Fig. 3(b)]. We denote the lower boundary of $\mathcal{U}(\bullet+^{\infty})$ outside $U(1)$ by E_+ and that between $U(1,s_0)$ and $S(1,s_0)$ by $E(0)$. $E(0)$ forms one piece of lower boundary for $\mathcal{U}(-\bullet+^{\infty})$, which is the part of $\mathcal{U}(\bullet+^{\infty})$ confined within $U(1)$. Obviously, each escape orbit must cross $\mathcal{U}(-\bullet+^{\infty})$ once and only once, which can then be looked at as the representatives for all escape orbits.

Denote $F^{-1}[E(0)]$ by $E(-1)$ [see Fig. 3(b)] which has two endpoints $S(1,s_0)$ and $S(2,s_0)=F^{-1}[S(1,s_0)]$ and represents a piece of the boundary of $\mathcal{U}(\bullet-+^{\infty})=F^{-1}[\mathcal{U}(-\bullet+^{\infty})]$. Discussion on the TECC orbits told us that $S(1,s)$ for $s\in[-s_1,1)$ share a common backward sequence $+^{\infty}-\bullet$. Noting that $s_0>-s_1$, we have

$$S(1,s_0)\in\mathcal{U}(+^{\infty}-\bullet)\subset\mathcal{U}(-\bullet) \quad \text{and}$$
$$S(2,s_0)\in\mathcal{U}(+^{\infty}\bullet-)\subset\mathcal{U}(+\bullet).$$

Therefore, the location of the two endpoints implies that $E(-1)$ must cross $U(1)$. The point of intersection must be $U(1,s_1)$, as it corresponds to the orbit that has a TECC and leads to critical escape after an additional e-e collision.

By acting the time reversal operation ($P\rightarrow -P$), E_+, $E(0)$, and $E(-1)$ are converted to I_-, $I(0)$, and $I(1)$ respectively [Fig. 3(b)]. The critical injection line $I_-\cup I(0)$ forms the upper boundary of the injecting region $\mathcal{U}(+^{\infty}\bullet)$ with $P=-\sqrt{2(Z-1)}$. $I(1)=F[I(0)]$ is a piece of the boundary for $\mathcal{U}(+^{\infty}-\bullet)$. The two end points of $I(0)$ are $S(1,-s_0)$ and $U(1,-s_0)$. Since $S(2,s_0)\in\mathcal{U}(+^{\infty}\bullet-)$ is below $I(0)$ and $-s_0<s_1$ implies that $U(1,s_1)$ is above $I(0)$, $I(0)$ must cross $E(-1)$. The crossing point corresponds to an orbit which begins with zero energy injection and ends in critical escape after one e-e collision, where we must have $r_1=r_2=1$ and $p_2=-p_1=\sqrt{2(Z-1)}$. Consequently, the point is unique and in Fig. 3(c) it is denoted by A. Since $I(1)$

has its lower end point $U(1,-s_0)$ and the upper end point $U(2,-s_0)=F[U(1,-s_0)]\in\mathcal{U}(-\bullet+^\infty)$, it in turn crosses $E(-1)$ at point B (located at $P=0$ and numerically found unique), $S(1)$ at point $S(1,-s_1)$ and $E(0)$ at point $A^*=F(A)$ [Fig. 3(c)].

Based on the above discussion, the resonant zone D on SOS can be defined as the complement of

$$\mathcal{U}(\bullet+^\infty)\cup\mathcal{U}(+^\infty\bullet)\cup\mathcal{U}(+^\infty-\bullet-+^\infty),$$

where $\mathcal{U}(+^\infty-\bullet-+^\infty)=\mathcal{U}(\bullet-+^\infty)\cap\mathcal{U}(+^\infty-\bullet)$. It is a symmetric region with respect to $P=0$ confined by the critical escape and injection curves. The upper boundary is $E_+\cup E(0)$ while the upper left one is part of $E(-1)$ from $S(1,s_0)$ to the point B. The boundary can be completed by adding the time reversal of the former two, i.e., $I_-\cup I(0)$ and a part of $I(1)$ from $U(1,-s_0)$ to point B. We further divide D into three parts, i.e., $D=D_I\cup D_B\cup D_O$ with $D_I=D\cap\mathcal{U}(+^\infty-\bullet)$, $D_O=D\cap\mathcal{U}(\bullet-+^\infty)$, and what remained is denoted by D_B. D_I is a trianglelike region. Its three edges are $E(0)$ from point A^* to $S(1,s_0)$, $E(-1)$ from $S(1,s_0)$ to point B, and a segment of $I(1)$ from point B to point A^*, respectively [Fig. 3(c)]. D_O is the time reversal of D_I. For a delayed scattering orbit, its symbolic sequence must be $+^\infty-\Sigma-+^\infty$, where Σ is a finite string of length k which describes its resonant motion. Then the orbit will consecutively cross D at $k+1$ points, the first and last of them are contained in D_I and D_O respectively while all the middle $k-1$ points are located within D_B. In this meaning, we say that D_I is the entrance while D_O is the exit of the resonant zone D. In addition, for a bounded orbit, all the points of intersection must be confined within D_B.

E. Horseshoe and partition of SOS

We are now ready to show the Smale horseshoe structure in the dynamics. To demonstrate the deformation of D_B under the action of F^{-1}, we fill $D_I\cup D_B$ with many fibers and see how they are changed by the map [Fig. 4(a)]. Each of these fibers satisfies that, (i) its one end is located at the lower boundary of D_B while another, for simplicity, is $S(1,s_0)$ so that it must cross $U(1)$ and (ii) the point of intersection is unique, which must be $U(1,s)$, $s\in[s_1,s_0]$. In a topologically deformed diagram of $D_I\cup D_B$ shown in Fig. 5(a), all those fibers as well as $S(1)$ vertically cross D_B while $U(1)$ horizontally cuts all the fibers. Under the action of F^{-1}, the points of intersection with $U(1)$ are now mapped to $S(1,s)$, $s\in[s_1,s_0)$, which can be regarded as the upper endpoints for the fibers of next generation [Fig. 5(c)]. In the meantime the upper endpoints of the primary fibers move into $\mathcal{U}(+^\infty\bullet-)$ [e.g., the point $S(1,s_0)$ is mapped to $S(2,s_0)$, see Fig. 4(b)], leading the fibers cross $I(0)$ and their points of intersection become the lower endpoints for the new fibers. Finally, the lower ends located at the lower boundary of D_B [i.e., $I(0)\cup I_-$] remain on it and they move rightward into I_- to make room for the newcomers [e.g., point A moves to point A', see Fig. 4(b)]. Note here that the fact $s_1\geqslant 0$ is crucial to guarantee all the new-generated fibers crossing D_B [see Fig. 5(d)]. Therefore, mapped by F^{-1}, one

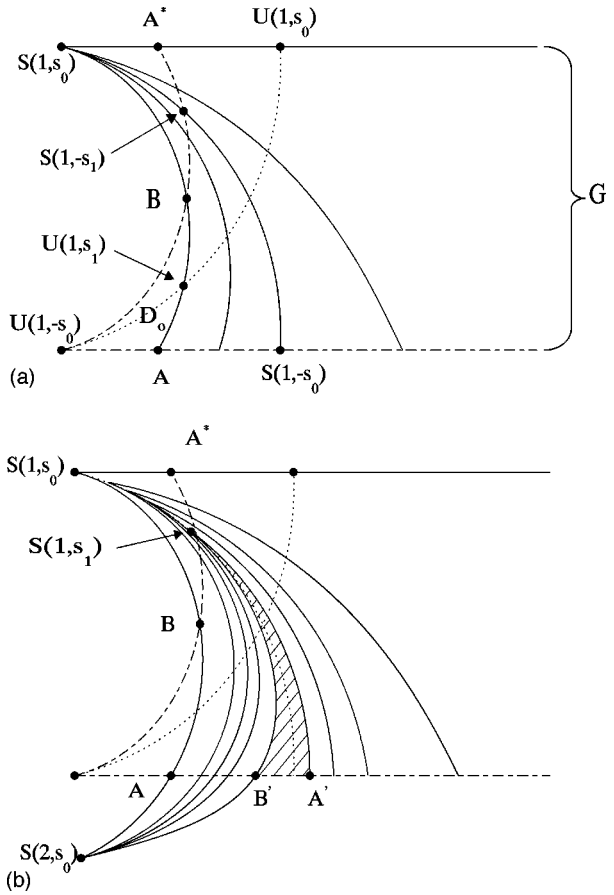

FIG. 4. The deformation of the fibers in D_B under the action of F^{-1}. Three representative fibers, $E(-1)$ from $S(1,s_0)$ to point A, $S(1)$ from $S(1,s_0)$ to $S(1,-s_0)$ and $E_+\cup E(0)$, which can be looked as meet I_- at infinity (point G), as well as two other fibers between them are shown in (a). Images of these five fibers mapped by F^{-1} are shown in (b). The shadowed area is $F^{-1}(D_O)$.

piece of fiber is split into two, which manifest the stretching and folding of D_B. In fact, it is topologically a smale horseshoe (Fig. 5).

For each piece of new generated fiber, we do not know whether or not it crosses $U(1)$ also at only one point. However, our numerical study shows that it is true for the sequential series of fibers generated from the primary fiber $S(1,s)$, $s\in[-s_0,s_0]$ by repeating the inverse Poincaré mapping F^{-1}. The fibers of the kth generation are actually segments of $S(k)=F^{-k+1}[S(1)](k\geqslant 1)$ included within $D_I\cup D_B$. Each segment of $S(k)$, e.g., $\mathcal{U}(\bullet\Sigma c)$, crosses $U(1)$ only at one point, by which it is divided into two parts $\mathcal{U}(-\bullet\Sigma c)$ [inside $U(1)$] and $\mathcal{U}(+\bullet\Sigma c)$ [outside $U(1)$]. These two parts are mapped by F^{-1} to $\mathcal{U}(\bullet-\Sigma c)$ and $\mathcal{U}(\bullet+\Sigma c)$, then become two pieces of $S(k+1)$. Therefore, $S(k)$ is made up from 2^{k-1} pieces, i.e., $\mathcal{U}(\bullet\Sigma c)$ with Σ exhaust all binary (contains only $+$ and $-$) sequences of length $k-1$ and each of them cuts $U(1)$ and yields a BCCO with code sequence $+^\infty-c\Sigma c-+^\infty$. Moreover, by the 2^k-1 pieces of partition lines $S(k')$, $1\leqslant k'\leqslant k$, 2^k cells is determined on SOS. As c can be regarded as the degenerated $+$ and $-$, the two cells on the both sides of the partition line $\mathcal{U}(\bullet\Sigma c)$ are $\mathcal{U}(\bullet\Sigma+)$ and $\mathcal{U}(\bullet\Sigma-)$, respectively. Therefore, $\mathcal{U}(\bullet\Sigma)\neq\phi$ for an arbitrary binary sequence Σ of length k, or the binary symbolic dynamics is complete.

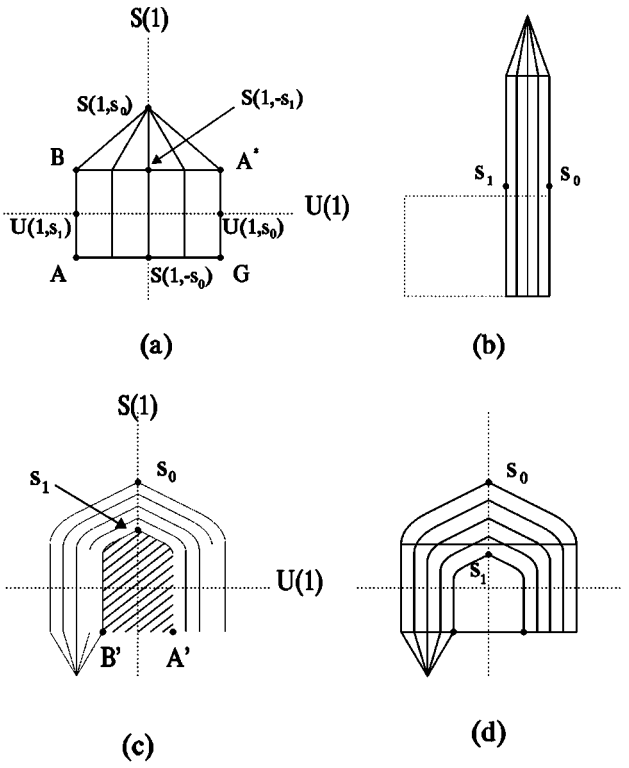

FIG. 5. Schematic diagram showing the horseshoe. (a) D_B (the rectangle ABA^*G) and five vertical fibers in it. Point G represents the edge of D_B at infinity. (b) Stretching. (c) Folding when $s_1>0$, the shadowed area is $F^{-1}(D_O)$. (d) Folding when $s_1<0$.

As each piece of partition line crosses $U(1)$ once and only once, we can give a natural order to the symbolic sequences such that $\Sigma_1<\Sigma_2$ if and only if $\mathcal{U}(\bullet\Sigma_1)$ crosses $U(1)$ at smaller s than that of $\mathcal{U}(\bullet\Sigma_2)$, where Σ_1 and Σ_2 are two arbitrary admissible sequences. The coarsest partition of SOS gives $-<c<+$. From the forgoing discussion on the deformation of $S(k)$ under the inverse Poincaré mapping, we know that adding a $+$ to a sequence will result in the stretching of the corresponding region while adding a $-$ will lead to an additional folding, so $+$ will preserve the order while $-$ will reverse it, i.e.,

$$\Sigma_1<\Sigma_2 \Rightarrow +\Sigma_1<+\Sigma_2 \text{ and } -\Sigma_1>-\Sigma_2,$$

which is the same as that in the one-dimensional unimodal map. Moreover, the well defined order for the complete set of symbolic sequences implies that the bounded motion in D_B is homeomorphic to the two-dimensional Baker's transformation.

F. Tilling of resonant zone by autoionization regions

We have seen that all BCCO's are scattering orbits. Actually, almost all initially bounded ($E_1,E_2<0$) motion will end in autoionization and it has been pointed out in Ref. [12] that the lifetime of the resonant motion imposes a fractal structure on phase space, leaving a cantor set for the (totally) bounded trajectories. Geometrically, this fact can be understood as the tilling of the resonant zone by the autoionization regions $F^{-k}(D_O), k>0$.

Consider the region $F^{-1}(D_O)$ [shadowed area in Fig. 4(b)]. It is an autoionization region, in which the code sequences for the escape orbits are $\bullet\sigma-+^{\infty}$, $\sigma=+,-,c$. Its upper end is $S(1,s_1)$ while the lower end is a line segment from $B'=F^{-1}(B)\in I(0)$ to $A'=F^{-1}(A)\in I_-$, which belongs to the lower boundary of D_B. Therefore, this striplike autoionization region, which contains the partition line $S(1,s)$, $s\in[-s_0,s_1)$, ''vertically'' crosses D_B and, as a result, will also be subjected to stretching and folding under the action of F^{-1}, just like the reduplication of the partition lines. Therefore, within $D_B\cup D_I$, the partition line $\mathcal{U}(\bullet\Sigma c)$ is enclosed by an autoionization region in which the sequences for the escape orbits are $\bullet\Sigma\sigma-+^{\infty}$, $\sigma=+,-,c$. Moreover, orbits start from both two edges of those striplike regions will lead to critical escape.

The completeness of symbolic dynamics indicates that there exist a great diversity of escaping patterns in the resonant zone. In fact, if we view the transformation of these autoionization regions in a time reversal version by making use of the reflection $P\rightarrow -P$, we will obtain a picture of the evolution of D_I (which can be regarded as the ensemble of the resonant scattering orbits), i.e., endless stretching and folding under the action of F while part of its orbits fall into D_O and escape away. When we take all those infinitely many striplike autoionization regions together with their time reversal (i.e., the resonant injection regions) away from D_B, the remaining set forms a fractal basin which gives the bounded motion.

G. Scattering orbits

A scattering orbit can be initiated as follows. The inner electron (e_2) is oscillating near the nucleus with fixed negative energy E_2^0 while the outer electron (e_1) is injecting from a sufficiently far distance with positive energy $E_1^0=-1-E_2^0$. As the two electrons are uncoupled before their first encounter, we can simply fix e_1 at a distance out of the amplitude of e_2 and scan the phase of e_2 so as to overview all scattering orbits for a given incident energy. The scattering functions are defined as the dependence of the final quantities, such as the final escape energy or the time of scattering, upon the initial state parameter, i.e., the phase of e_2.

Immediately before the first e-e collision, the incident orbits must cross SOS within the region $\mathcal{U}(+^{\infty}\bullet-)$ and these representative points can be looked as the injection ensemble. Since the scaling symmetry of Coulomb systems implies that the behavior of scattering orbits at an arbitrary negative total energy depends only on the scaled incident energy $\varepsilon_i\equiv E_1^0/|E_2^0|\in(0,1)$, it is convenient to organize the points in the injection ensemble into incident curves according to different ε_i and denote each incident curve by

$$I(\varepsilon_i,0)=\left\{(R,P)\in\mathcal{U}(+^{\infty}\bullet-)\,\middle|\,P=-\left[2\left(Z-1+\frac{\varepsilon_i}{1-\varepsilon_i}R^2\right)\right]^{1/2}\right\}.$$

When $\varepsilon_i\rightarrow 0$, $I(\varepsilon_i,0)$ will approach $I(0)$, the critical injection line. With the increase of ε_i, $I(\varepsilon_i,0)$ moves leftward and tends to the boundary $R=0$ when $\varepsilon_i\rightarrow 1$ (Fig. 6).

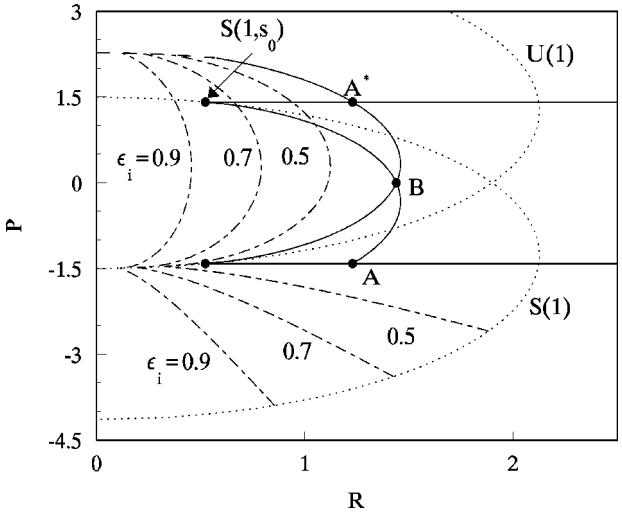

FIG. 6. $I(\varepsilon_i,0)$ and $I(\varepsilon_i,1)$ (dashed lines) with $\varepsilon_i=0.9$, 0.7, and 0.5 from left to right. The resonant zone is bounded by solid lines.

After one more crossing of SOS, the injection ensemble arrives $\mathcal{U}(+^{\infty}-\bullet)$ which are filled with incident curves $I(\varepsilon_i,1)=F[I(\varepsilon_i,0)]$. By the partition line $S(1,s)(s>s_0)$ and the critical escape curves $E(0)$ and $E(-1)$ [from point A^* to $S(1,s_0)$ then to point B], $\mathcal{U}(+^{\infty}-\bullet)$ is divided into three parts. The uppermost one is its intersection with $\mathcal{U}(-\bullet+^{\infty})$ where the orbits will end in undelayed exchange scattering with code sequence $+^{\infty}-+^{\infty}$ while the lowermost one is confined within $\mathcal{U}(\bullet-+^{\infty})$ where the orbits will give direct scattering coded by $+^{\infty}--+^{\infty}$. The middle part is D_I, with the cusp at $S(1,s_0)$ delimited by $E(0)$ and $E(-1)$, where the orbits will start their resonant motion. Note that not all incident curves can intersect with D_I. If ε_i is too large, the curve will cut $S(1)$ at $S(1,s)$ with $s>s_0$ and not cross D_I. Consequently, the scattering contains only undelayed ones and is as regular as that in the case of $E\geqslant 0$. Transition takes place at $\varepsilon_i=\varepsilon_{ic}\approx 0.809417$ when the curve $I(\varepsilon_i,1)$ passes $S(1,s_0)$. If $\varepsilon_i<\varepsilon_{ic}$, $I(\varepsilon_i,1)$ will cut D_I and the scattering will be complicated by the resonant motion. As D_I are tilled by infinitely many striplike autoionization regions, the intersection between $I(\varepsilon_i,1)$ and D_I implies that there are infinitely many patterns of resonant motion for the scattering orbits with fixed $\varepsilon_i<\varepsilon_{ic}$ which will result in a chaotic band in the scattering function. Furthermore, the intersection of $I(\varepsilon_i,1)$ with all autoionization regions will result in a hierarchy of infinitely many regular (continuous) islands within the chaotic band (Fig. 7).

With the decrease of ε_i, the incident curve will move rightward and intersect with more and more partition lines, leading to more and more possible patterns of resonance motion. The permitted forward sequences for the incident orbits at a given ε_i can be determined as follows. Consider the point where $I(\varepsilon_i,1)$ crosses $S(1)$. It corresponds to an outgoing TECC orbit, which we shall call the *principal TECC orbit* of the ensemble with incident energy ε_i. Assume the forward sequence for the principal TECC orbit is $c\Sigma$. Then the possible forward sequences for this ensemble are $+\Sigma'$, which is larger than $+\Sigma$, and $-\Sigma'$, which is less than $-\Sigma$. In both cases, we have $\Sigma'\geqslant\Sigma$ (see Fig. 8). Σ arrives at its minimum, i.e., $-+^{\infty}$, when the incident curve cuts $S(1)$ at

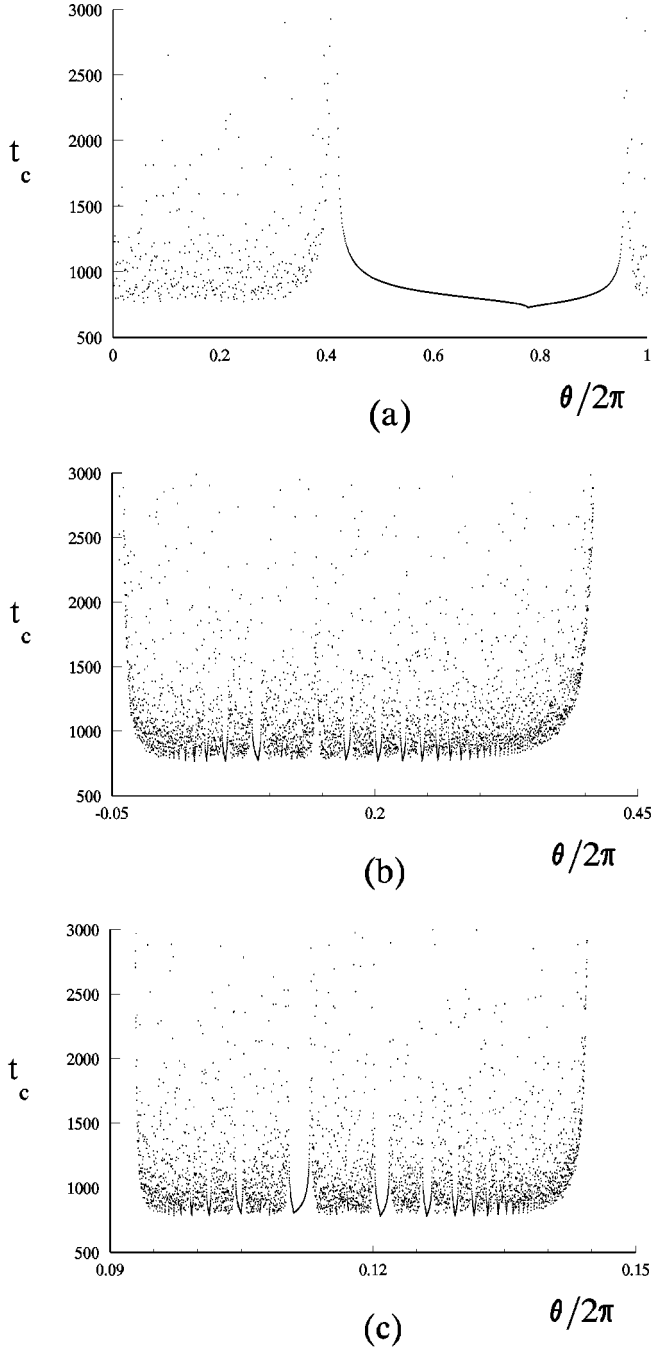

FIG. 7. (a) Scattering time (defined as the lifetime of the state satisfying $r_1,r_2<100$) vs initial phase of the inner electron θ. The incident energy ϵ_i is set as 0.01. (b) Enlargement of chaotic band of (a). (c) Enlargement of the first left-hand side chaotic band of the central regular island of (b). This structure of self-similarity resembles that which has been observed in collinear $e^-+\mathrm{He}^+$ chaotic scattering [11], except for the fact that the tips of the cusp-shaped regular islands correspond here to TECC rather than triple collision orbits.

$S(1,s_1)$ where we have $\varepsilon_i=\varepsilon_{ic}'\approx 0.043317$. When $\varepsilon_i\leqslant\varepsilon_{ic}'$, $I(\varepsilon_i,1)$ will cut all partition lines and, consequently, there is no restriction to the forward (binary) sequences for the scattering orbits.

In the initial incident ensemble of fixed ε_i, if e_2 is equally spaced distributed according to its angle variable

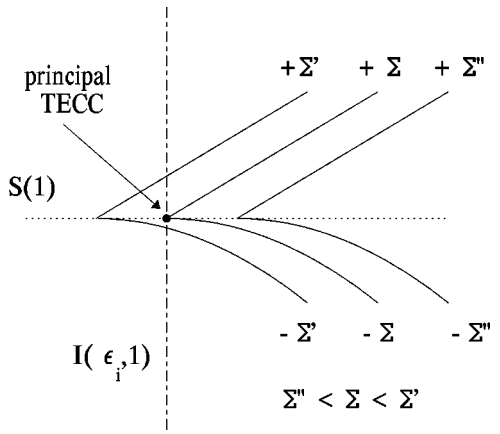

FIG. 8. Schematic diagram to show how the incident curve $I(\varepsilon_i,1)$ cuts the partition lines (solid curves).

then the classical probability for the resonant scattering $P_{\rm res}$ can be obtained by calculating the portion of $I(\varepsilon_i,1)$ which are fallen into D_I. The dependence of $P_{\rm res}$ on ε_i are shown in Fig. 9. It can be shown that, at $S(1,s_0)$, $E(0)$ intersects $S(1)$ at a finite (nonzero) angle while $E(-1)$ is tangential to $S(1)$. Therefore, immediately below the threshold ε_{ic}, $P_{\rm res}$ increases linearly with $\varepsilon_{ic}-\varepsilon_i$.

IV. DISCUSSION

We pointed out in Sec. III E that the existence of the smale horseshoe relies on the fact that all incoming TECC will lead to immediately ionization after an additional *e*-*e* collision, or $s_1 \geqslant 0$. This fact persists for $Z \in (1,Z_c]$ with $Z_c \approx 2.348086$. If $Z>Z_c$, we have $s_1<0$ which implies that $F(D_I)\cap D_o=\phi$. In this underdeveloped smale horseshoe, some binary code sequences, for example $+^{\infty}-+-+^{\infty}$, are forbidden. By taking the nuclear charge as unit, we can rewrite the Hamiltonian as

$$H_\delta=\frac{1}{2}(p_1^2+p_2^2)-\frac{1}{r_<}-\frac{1-\delta}{r_>},$$

with $\delta=1/Z$. One can then naturally expect that with the decrease of δ, more and more symbolic sequences will be truncated until an integrable system is arrived at $\delta=0$. The weakening of chaos with the increase of Z has also been justified in calculating the uncertainty dimension for a fractal set generated by autoionization on phase space [14]. Numerical explorations on phase space show that the system remains purely hyperbolic, i.e., has no stable island and invariant tori even when $\delta \approx 0_+$. This is of course not contradicted with KAM theorem as H_δ is not smooth and, maybe more serious, has a singularity at $r_1=r_2=0$. In tracing periodic orbits (PO's) with δ tending to zero, we find they behave in two typical ways. For the PO's which are permitted by H_0, their instability decreases with δ and at $\delta=0$ they become marginal (parabolic) stable. Actually, a bifurcation takes place at $\delta=0$ and all those PO's will be stable if δ passes this point. For the PO's which are forbidden by H_0, they will either die before $\delta=0$ due to the occurrence of TECC or become singular due to the collision with the origin and disappear at $\delta=0$. The latter case is reasonable if we notice that the existence of those strongly coupled orbits depends on an effective redistribution of E to E_1 and E_2, which can only be realized at $r_1=r_2\simeq 0$ when δ is very small. On the other hand, the dynamics at the limit $Z\to 1$ is more simple. Note that the resonant zone is delimited by $P=\pm\sqrt{2(Z-1)}$, which will shrink to zero if Z decreases to 1, when $Z<1$ there exists no more recurrent motion.

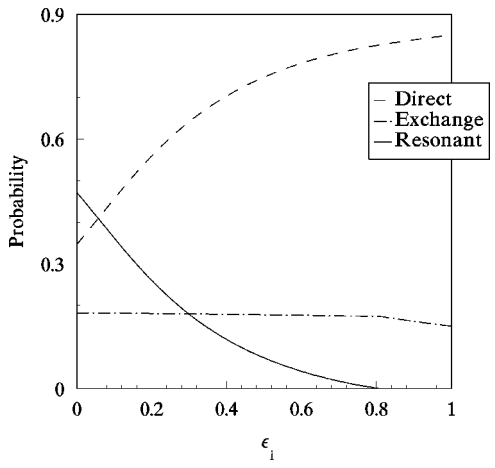

FIG. 9. Probability for undelayed direct, undelayed exchange, and resonant scatterings as functions of incident energy ε_i.

In *s*-wave helium, the electron-electron interaction has been adopted in a spherically averaged form while its dynamics closely resembles that of the e^-Ze^- collinear helium in which the repulsive interaction between the electrons is minimized [4]. In both systems we can see purely chaotic bounded motion with a complete binary symbolical description and chaotic scattering which can be better related to critical escape rather than unstable periodic orbits [4,11]. This resemblance reflects the common physics of the three-body Coulomb system resulted from its long range and singular interaction. Nevertheless, there exist some remarkable differences between these two systems, which are directly related to the fact that a smooth electron-electron interaction is adopted in the latter system. In e^-Ze^- collinear helium, the collision of an orbit with the singularity at $r_1=r_2=0$ cannot always be avoided as that in *s*-wave helium. In fact, the global dynamics of the collinear helium is drastically dominated by this singularity of triple collision. Affected by the singularity, the completeness of binary symbolic dynamics persists for $Z>Z_1\approx 0.2877742$ and the escape energy is not bounded for its scattering orbits [17]. In this sense, we say that the collinear helium is more chaotic than *s*-wave helium. Moreover, the threshold behaviors in the two systems are qualitatively different. In the collinear helium, it has been found that the channel for $(e,2e)$ reaction (or chaotic scattering) is open when E is above (or below) the threshold at zero and the probability of the reaction as the function of the energy deviation obeys the well-known ''Wannier's power law'' near $E=0$ [10]. As the existence of the Wannier threshold law in $(e,2e)$ scattering had been confirmed by experiments [20], it is reasonable to believe that the e^-Ze^- collinear helium describes the correct threshold behavior of the real helium. On the contrary, in the *s*-wave helium, even for $Z>Z_c$, the $(e,2e)$ reaction (or chaotic scattering) only occurs when E is above (below) a positive(negative) threshold and near the threshold the increase of the probability

obeys a linear law. These inappropriate results, which had also observed in the quantum calculation [16], are physically attributed to the lack of angular correlation between the two electrons due to their restriction to *s*-wave states. We shall here give a dynamical explanation of this difference. It has been long realized that the motions near the symmetric stretching of the two electrons on the opposite sides of the nucleus (i.e., the Wannier ridge) play an important role in the three-particle break up at small $E>0$ [19]. On the other hand, numerical experiments on chaotic scattering in e^-Ze^- collinear helium show that all resonant orbits are initiated from the nearly symmetric outgoing electron pair. These facts indicate that the Wannier type motions are crucial to the excitation of resonance (for $E<0$) or ionization (for $E>0$) in real helium. However, in *s*-wave helium, as we have mentioned, the symmetric motion on the Wannier ridge is excluded by the dynamics. Therefore, it cannot give a proper description of the motion near the threshold. Despite those differences in classical dynamics, as the singularity of triple collision might lose its importance in quantum description due to the uncertainty principle, it is expected that simple *s*-wave helium will stand as a useful model in studying the quantum chaology, rather than the threshold behavior, in the three-body Coulomb system.

V. SUMMARY

In our study of the classical dynamics of *s*-wave helium, we first introduce the motion in FD so as to eliminate the discontinuity at TECC. The resonant (chaotic) scattering orbits are distinguished by the delay due to the recurrence of reaction. Based on the qualitative behavior of the TECC orbits, the resonant zone on SOS is explicitly defined which is delimited by the critical injection and escape curves. For $Z=2$, a Smale horseshoe can be constructed in the Poincaré mapping and, consequently, the binary symbolic dynamics is complete. We show that the resonant zone is tilled by infinitely many striplike autoionization regions surrounding the partition lines. The bounded motion, which occurs on a cantor set in the phase space, is purely chaotic. The intersection of incident ensemble with the resonant zone, which takes place when the incident energy is below a threshold, marks the onset of chaotic (resonant) scattering. The symbolic sequences for possible resonant motion at a given incident energy are determined by the principal TECC orbit. Immediately below the threshold, the probability for resonant scattering as a function of the excess energy follows a linear law.

ACKNOWLEDGMENTS

This work was supported by the Nonlinear Science Project of the Climbing Program for Fundamental Research.

APPENDIX: TECC ORBITS WHEN $S\to 1$

Let $(R_i,P_i)=(\sqrt{r_i},\sqrt{r_i}p_i)$ for $i=1,2$, then the dynamical equations read

$$\frac{dR_i}{dt}=\frac{P_i}{2R_i^2},\quad \frac{dP_i}{dt}=\frac{E_i}{R_i},\quad i=1,2,$$

from which we have

$$\frac{dP_1}{dP_2}=\frac{R_2E_1}{R_1E_2}.$$

If an orbit has a TECC at $t=t_c$, then

$$[R_1(t_c),P_1(t_c)]=[R_2(t_c),P_2(t_c)]=\sqrt{2Z-1}(\sqrt{1-s^2},s)\equiv[\sqrt{\rho(s)},P_c(s)],\quad s\in(-1,1).$$

Assume its two nearest crossings of SOS to the TECC occur at $t=t_1$ and t_2, $t_1<t_c<t_2$, i.e.,

$$[R_2(t_1),P_2(t_1)]=[R_2(t_2),-P_2(t_2)]=(0,\sqrt{2Z}).$$

According to the definition, we have

$$S(1,s)=[R_1(t_1),P_1(t_1)]\ \text{ and }\ U(1,s)=[R_1(t_2),P_1(t_2)].$$

If $s>s_0=\sqrt{(2Z-2)/(2Z-1)}$, which implies $E_1>0$, then dR_1/dt, $dP_1/dt>0$ and we have

$$R_1(t_1)<\sqrt{\rho(s)}<R_1(t_2),$$
$$\sqrt{2(Z-1)}<P_1(t_1)<P_c(s)<P_1(t_2),$$

and

$$P_1(t_2)=P_c(s)+\int_{P_c(s)}^{-\sqrt{2Z}}\frac{R_2E_1}{R_1E_2}dP_2=P_c(s)+\int_{-\sqrt{2Z}}^{P_c(s)}\frac{R_2E_1}{R_1|E_2|}dP_2<2P_c(s)+\sqrt{2Z}.$$

When $s\to 1$, we have $R_1(t_1)<\sqrt{\rho(s)}\to 0$. Moreover, $P_1(t_2)<+\infty$ and $E_1(s)\to+\infty$ imply also $R_1(t_2)\to 0$. If $P_1(t_1)\to P'$ and $P_1(t_2)\to P''$, then

$$S(1,s)\to(0,P')\ \text{ and }\ U(1,s)\to(0,P''),$$

with

$$\sqrt{2(Z-1)}<P'<\sqrt{2Z-1}<P''<2\sqrt{2Z-1}+\sqrt{2Z}.$$

[1] S. Wantanabe, Phys. Rev. A **36**, 1566 (1987).
[2] K. Richter and D. Wintgen, J. Phys. B **23**, L197 (1990).
[3] G. S. Ezra, K. Richter, G. Tanner, and D. Wintgen, J. Phys. B **24**, L413 (1991).
[4] D. Wintgen, K. Richter, and G. Tanner, Chaos **2**, 19 (1992).
[5] K. Richter, G. Tanner, and D. Wintgen, Phys. Rev. A **48**, 4182 (1993).
[6] R. Blümel and W. P. Reinhardt, in *Quantum Nonintegrability*,

Vol. 4 of *Direction in Chaos*, edited by D. H. Feng and J. M. Yuan (World Scientific, Singapore, 1992).
[7] P. Gaspard and S. A. Rice, Phys. Rev. A **48**, 54 (1993).
[8] T. Yamamoto and K. Kaneko, Phys. Rev. Lett. **70**, 1928 (1993).
[9] J. M. Yuan and Y. Gu, Chaos **569** 3 (1993); Y. Gu and J. M. Yuan, Phys. Rev. A **47**, R2442 (1993).
[10] J. M. Rost, J. Phys. B **27**, 5923 (1994).
[11] X. Tang, Y. Gu, and J. M. Yuan, Phys. Rev. A **54**, 496 (1996).
[12] G. Handke, M. Draeger, and H. Friedrich, Physica A **197**, 113 (1993).
[13] G. Handke, M. Draeger, W. Ihra, and H. Friedrich, Phys. Rev. A **48**, 3699 (1993).
[14] G. Handke, Phys. Rev. A **50**, R3561 (1994).
[15] M. Draeger, G. Handke, W. Ihra, and H. Friedrich, Phys. Rev. A **50**, 3793 (1994).
[16] W. Ihra, M. Draeger, G. Handke, and H. Friedrich, Phys. Rev. A **52**, 3742 (1995).
[17] Z.Q. Bai, Y. Gu, and J.M. Yuan, Physica D **118**, 17 (1998).
[18] A. Tiyapan and C. Jaffe, J. Chem. Phys. **103**, 5499 (1995).
[19] G. Wannier, Phys. Rev. **90**, 817 (1953).
[20] J. W. McGowan and E.M. Clarke, Phys. Rev. **167**, 43 (1967).